International Journal of Computer Vision 19(3), 289–300 (1996)

Sub-Pixel Bayesian Estimation of Albedo and Height*

HASSAN SHEKARFOROUSH, MARC BERTHOD AND JOSIANE ZERUBIA
INRIA–2004 Route des Lucioles, 06902 Sophia Antipolis Cedex, France

MICHAEL WERMAN
Institute of Computer Science, Hebrew University of Jerusalem, 91904 Jerusalem, Israel

Received December 30, 1993; Accepted May 30, 1995

Abstract. Given a set of low resolution camera images of a Lambertian surface, it is possible to reconstruct high resolution luminance and height information, when the relative displacements of the image frames are known. We have proposed iterative algorithms for recovering high resolution albedo with the knowledge of high resolution height and vice versa. The problem of surface reconstruction has been tackled in a Bayesian framework and has been formulated as one of minimizing an error function. Markov Random Fields (MRF) have been employed to characterize the a priori constraints on the solution space. As for the surface height, we have attempted a direct computation without refering to surface orientations, while increasing the resolution by camera jittering.

1. Introduction

Image resolution depends on the physical characteristics of the sensor: the optics, the density and the spatial response of the sensing elements. Increasing the resolution by sensor modification may not always be an available option. An increase in the sampling rate can, however, be achieved by obtaining more samples of the same scene from a sequence of displaced images.

In this paper we propose an algorithm for reconstructing high resolution images given a set of low resolution observations. Markov Random Field's (MRF) (Azencott, 1987; Besag, 1974, 1986) have been used for modeling the *a priori* information on images. Use of MRF which became popular with the ingenious paper of Geman and Geman (1984) is indeed equivalent to regularization techniques used by Marroquin et al. (1987), Terzopoulos (1986), Grimson and many others (see Keren and Werman, 1993). Therefore, in what follows, MRF's will be directly interpreted in terms of regularization.

*This project was partially supported by AFIRST (l'Association Franco-Israelienne pour la Recherche en Science et en Technologie).

We propose, below, to work on some fundamental applications of optimization in the field of surface reconstruction. There is, for example, an extensive literature on extracting 3D information, which is based mainly on stereopsis and motion analysis (Prager et al., 1983). Herein, we intend to investigate the possibility of direct retrieval of 3D high resolution visual information from a sequence of displaced low resolution intensity images.

Early research on super-resolution was carried out by Tsai and Huang (1984), who used frequency domain methods, disregarding the blurring effect of the imaging process. Later, Gross (1986) assumed an exact knowledge of the imaging process and the relative shifts between the input pictures. He then constructed a single blurred picture of higher spatial sampling rate by merging the low resolution images over a finer grid using interpolation. The merged picture was then deblurred by means of a restoration filter using standard pseudo-inverse techniques applied to the blurring operator. As in the work of Tsai and Huang, only interframe translations were considered.

Peleg et al. (1987, 1989) estimated an initial guess of the higher resolution image, and simulated the imaging

process to obtain a set of estimated low resolution camera images. Using an error criterion based on the difference between the estimated and actual sensor images they devised an iterative algorithm to reconstruct the higher resolution image. The method however suffered from lack of speed and sensitivity to noise. Irani and Peleg (1989, 1991) describe a method based on the resemblance of the presented problem to the reconstruction of a 2D object from its 1D projections in Computer Aided Tomography (CAT). The high resolution image is constructed using an approach similar to the back-projection method used in CAT.

Herein, we will assume a quite general reflectance model and hence the formulation shares common points with that of height from shading (Horn, 1989; Leclerc and Bobick, 1991). Future extensions may include other reflectance laws. We will also look at different optimization algorithms. Tests have been carried out on both synthetic and real data.

2. Lambertian Image Formation

In this section, we will recall the model for computing the irradiance for a Lambertian surface. Rigorous analyses of this problem were first carried out by Horn in early 70's (1970, 1977). Horn introduced optical models of image acquisition in the area of computational vision which were based on projecting surface points onto the image plane.

The basic underlying assumption for a Lambertian surface is that brightness variations depend, in a deterministic way, on physical properties of the scene: the light intensity is dependent on the surface albedo and the surface orientation. Therefore, the luminance energy G can be determined by Lambert's law (Wolff et al., 1992):

$$G \propto g \cos(i) \tag{1}$$

where g is the surface albedo and i is the incident angle. The proportionality factor is the incident illumination intensity which for a uniform illumination of the surface can be considered as being constant.

It can be seen from this simple formula that, photometrically, an infinite number of albedo and orientation combinations can lead to the same image light intensity. Therefore, recovering surface characteristics and structures is an underconstrained problem and requires additional constraints for solution. On the other hand, one can also assume that invariant pictorial features (e.g., regions of homogeneous brightness) correspond to semantically meaningful objects or surfaces of objects. The latter can be considered as an *a priori* information or a constraint which is usually imposed in terms of smoothness. This means that brightness variations are usually smooth and depend on underlying physical phenomena of the outside world. The exceptions to this are the boundary discontinuities, which can cause brightness edges.

2.1. Proposed Imaging Model

We shall, henceforth, assume that our sensor is a pinhole camera located far enough from the observed surface so that the projection of any surface point on the retina of the camera can be regarded as being orthographic. Moreover, camera parameters will be assumed to be known.

As for the surface, we shall, hereafter, sample it into a two dimensional array and represent the surface albedo by $g(x, y)$ and the 3D graph of the surface by $z(x, y)$.

In our imaging model, we will also included a point spread function (PSF) (Andrews and Hunt, 1977; Rosenfeld and Kak, 1982) and therefore, our irradiance equation will differ slightly from the standard one given above, i.e., the image intensity is formed by convolving the luminance energy in an area around a point on the surface with the PSF kernel whose size and form depends on the sensors being used. For simplicity, this area is assumed to be a square window and its size depends on the spatial response of the sensor. Assuming that the PSF consists of a square window of area w and is of a Gaussian form, the camera image intensity at any pixel (k, l) is given by:

$$I(k, l) = \sum_{(x,y)\in w} H_w(x - x_c, y - y_c)\, g(x, y) R(x, y) \tag{2}$$

where $I(k, l)$ is the image intensity at image coordinates (k, l), $H_w(x - x_c, y - y_c)$ is the Gaussian kernel of support area w shifted by (x_c, y_c) and $R(x, y)$ is the Bi-Directional Reflectance Function (BDRF) of the surface, whose product with the albedo $g(x, y)$ yields the luminance energy reflected from coordinates (x, y) in the high resolution array. $R(x, y)$ is a function of the normal to the surface $\vec{n}(p_{xy}, q_{xy}, -1)$ (Berthod et al., 1993):

$$R(x, y) = \frac{\langle \vec{n}, \vec{\ell} \rangle \langle \vec{n}, \vec{s} \rangle}{\sqrt{p_{xy}^2 + q_{xy}^2 + 1}} \tag{3}$$

where $\langle .,. \rangle$ specifies the scalar product of two vectors, $p_{xy} = \frac{\partial z(x,y)}{\partial x}$, $q_{xy} = \frac{\partial z(x,y)}{\partial y}$ and $\vec{\ell} = (\ell_x, \ell_y, \ell_z)$ and $\vec{s} = (s_x, s_y, s_z)$ are the unit vectors along the light source and the camera, respectively.

As for $H_w(x, y)$, it is given by a 2D Gaussian kernel of the form:

$$H_w(x, y) = \frac{1}{2\pi\sigma^2} \exp\left(-\frac{x^2 + y^2}{2\sigma^2}\right) \tag{4}$$

where σ is the standard deviation of the kernel depending on focusing features of the camera.

Camera coordinates (k, l) are related to the world coordinate frame by:

$$k = a_{11}x + a_{12}y + a_{13}z + a_{14} \tag{5}$$

$$l = a_{21}x + a_{22}y + a_{23}z + a_{24} \tag{6}$$

Assuming that camera motions from one frame to another are only composed of translation and rotation around the origin of the world coordinate frame (De Castro and Morandi, 1987):

$$a_{11} = a_{22} = S_x \cos\theta \tag{7}$$

$$-a_{12} = a_{21} = S_y \sin\theta \tag{8}$$

where S_x and S_y are the relative sampling rates of the camera along x and y axes, respectively, and θ is the rotation angle of the camera around the origin of the world frame. Working on square images of widths d and D for the low resolution and the high resolution frames, respectively, and assuming uniform and equal sampling rates along both axes, we have: $S_x = S_y = \frac{d}{D}$. As for other camera parameters, we have set $a_{13} = a_{23} = 0$ and a_{14} and a_{24} depend on the translation of the camera along the two axes. The latter should be in such a way that sub-pixel overlap is obtained between pixels of any two observed images in the sequence. This is sometimes refered to as camera jittering (Hutber, 1987).

3. A Probabilistic Framework

We can, now, formulate the problem as that of solving Eq. (2) which is a special case of the image irradiance equation (Horn, 1977). It is obvious that the problem at hand is an inverse one and is ill-posed (Tikhonov and Arsenin, 1977). On the other hand, there are several complications involved in the present problem. It is easy, for instance, to verify that the matrix equation corresponding to Eq. (2) is rank deficient, unless further equations are obtained by taking a sequence of frames of the same scene, and provided that the sequence of image frames are independent, i.e., obtained by camera jittering.

Another major difficulty is the multiplicity of the solution due to ill-posedness. A brief review of this issue can be found in Bruss (1982), Frankot and Chellappa (1988). The approach usually adopted in mathematical terms is to impose constraints on the solution space to limit the size of the set of possible solutions (Marroquin et al., 1987). This may involve certain *a priori* assumptions about the problem (such as surface characteristics, in our case) and hence one may require different degrees of constrainment on the solution space, depending on the problem to be solved or even during different stages of the same problem if it is being solved by an iterative method.

We have imposed a smoothness constraint for solving (2) and have adopted a Bayesian framework which leads to formulating the problem as one of maximising the posterior density function (i.e., Maximum a Posteriori (MAP) estimator (Rosenfeld and Kak, 1982)). A nice feature of this approach is that the objective function will usually reduce to sum of two sets of terms which characterize the faithfulness to observed data and the constraint on the solution space (i.e., the regularising term). As for the image frames we have used a markovian model which enables us to characterize the *a priori* information by the Gibbs energy of the associated field.

Let g and z denote the vectors of unknown variables i.e., the vectors of all $g(x, y)$ and $z(x, y)$, respectively. Let also $I^1 \cdots I^m$ denote the vectors of observed low resolution image frames. Then using Bayes law:

$$p(g, z \mid I^1 \cdots I^m) = Kp(I^1 \cdots I^m \mid g, z)\ p(g, z) \tag{9}$$

where K is a constant independent of g and z and $p(g, z)$ is their joint probability distribution.

Assuming that g and z are two independent variables:

$$p(g, z \mid I^1 \cdots I^m) = Kp(I^1 \cdots I^m \mid g, z)\ p(g)p(z) \tag{10}$$

According to the Hammersley-Clifford theorem (Moussouris, 1974) a MRF can be characterized by a Gibbs distribution. Below, we will assume a Gaussian MRF and hence:

$$p(g) = \frac{1}{Z_g} \exp\left(-u_g^T C_g^{-1} u_g\right) \tag{11}$$

and:

$$p(z) = \frac{1}{\mathcal{Z}_z}\exp\left(-u_z^T C_z^{-1} u_z\right) \tag{12}$$

where $\mathcal{Z}_g$ and $\mathcal{Z}_z$ are some normalizing constants, u_g and u_z are vector functions of local potentials of the associated fields and C_g and C_z are the covariance matrices of g and z, respectively.

Let now e denote the vector of observation error of $I^1 \cdots I^m$ for given g and z. Then, assuming a Gaussian distribution for e yields the following conditional density (Rosenfeld and Kak, 1982; Andrews and Hunt, 1977):

$$p(I^1 \cdots I^m \mid g, z) = \frac{1}{((2\pi)^{D^2} \mid C_e \mid)^{\frac{1}{2}}}\exp\left(-\frac{1}{2}e^T C_e^{-1} e\right) \tag{13}$$

where C_e is the covariance matrix of the error vector, and $\mid C_e \mid$ is its determinant.

Using the Maximum a Posteriori (MAP) estimator, which is simply the maximiser of the logarithm of the posterior density function, yields the corresponding cost function $E(g, z)$ as the sum of quadratic forms:

$$\begin{aligned} E(g, z) &= -\ln p(g, z \mid I^1 \cdots I^m) \\ &= e^T C_e^{-1} e + u_g^T C_g^{-1} u_g + u_z^T C_z^{-1} u_z \\ &\quad + \text{constant} \end{aligned} \tag{14}$$

We can, therefore, maximise the posterior probability distribution by minimising $E(g, z)$ which implies minimising the mean square error of the observation under a priori constraints imposed by $p(g)$ or $p(z)$. Using a membrane model (Blake and Zisserman, 1987) and assuming that the components of e are given by the absolute error $I^r - \hat{I}^r$, $r = 1 \cdots m$ (where $\hat{I}^r$ is the estimated vector of the rth observed frame), we can write the following cost function at any point (x, y) of our sampled array:

$$\begin{aligned} E_{(x,y)} = &\sum_{r=1}^{m} \sum_{(k',l') \in \vartheta_{(k,l)}} \frac{(I^r(k', l') - \hat{I}^r(k', l'))^2}{2\sigma_e^2} \\ &+ \sum_{(x',y') \in \nu_{(x,y)}} \frac{(\hat{g}(x, y) - \hat{g}(x', y'))^2}{2\sigma_g^2} \\ &+ \sum_{(x',y') \in \nu_{(x,y)}} \frac{(\hat{z}(x, y) - \hat{z}(x', y'))^2}{2\sigma_z^2} \end{aligned} \tag{15}$$

where k and l are as before given by Eqs. (5) and (6), $\vartheta_{(k,l)}$ is the set of all pixels in observed frames whose intensity is affected by the irradiance at (x, y), $\nu_{(x,y)}$ is the neighbourhood structure depending on the order of the MRF associated with g and z (we have assumed the same order for both g and z), σ_e^2, σ_g^2 and σ_z^2 are the variances of the error vector, g and z, respectively, and m is the number of observed camera images.

Note that the first term is a measure of the faithfulness to observed data while the other terms represent smoothness constraints on g and z. Note also that (15) is obtained by approximating the covariance matrices as being diagonal, with constant terms on the diagonal.

4. An Algorithm for Super-Resolution

The algorithm is iterative and is shown schematically in Fig. 1 (see Berthod et al., 1993, 1994).

We proceed as follows: we first initialize using a set of low resolution images with pixels on each frame registered at subpixel accuracy. The imaging process is then simulated to create a set of low resolution estimates of sensor observations. The objective function in (14) characterizing the estimation error and the Gibbs energy of our MRF's is minimised with respect to g or z. The algorithm is repeated iteratively until no more reduction in the objective function is achieved for a preset number of successive iterations.

4.1. *Computational Considerations*

Due to non-linearities involved in image formation one can easily see that the cost function in (14) may not be

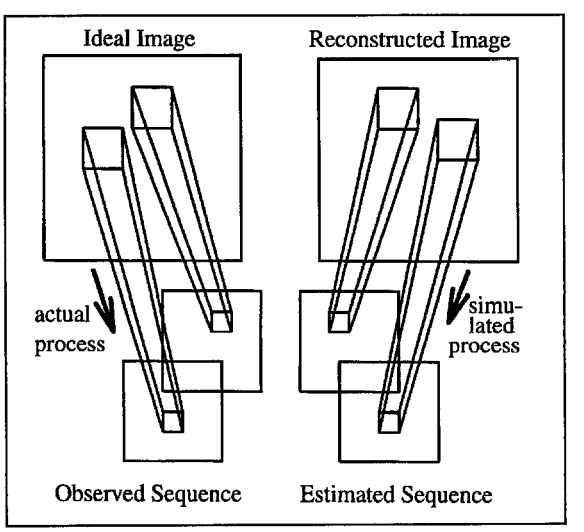

Figure 1. Schematic diagram of the algorithm.

easy to minimize. Two important issues to be considered are the scale of the dimension of the problem (even for small images), and the non-convexity. The former favours the choice of an optimization approach to a closed form solution. It is easy to verify that (14) will become convex for $\hat{g}$ when $\hat{z}$ is known. Therefore, one can obtain the solution using, for example, the Newton's Method. However the opposite is not true, i.e., the cost function is not convex for $\hat{z}$.

The non-convexity of the cost function for $\hat{z}$ can be tackled by means of some stochastic or deterministic optimization techniques such as the Simulated Annealing (SA) (Geman and Geman, 1984), the Mean Field Annealing (MFA)(Geiger and Girosi, 1991; Zerubia and Chellappa, 1993) or the Graduated Non-Convexity (GNC) (Blake and Zisserman, 1987). SA which can be applied to discrete variables, allows for random increase of the cost function so that one can escape local minima. The cost is, however, usually very high in terms of the computational time. GNC is relatively more attractive, but can be applied only when certain conditions are satisfied by the cost function. MFA is an alternative deterministic approach which does not necessarily lead to the optimal solution. One can, obviously, obtain the solution by using gradient based methods, if the algorithm is initialized near the solution. Herein, we propose a method described in Section 4.2.

To apply Newton's method we need to compute the partial derivatives of E with respect to $\hat{g}$ and $\hat{z}$:

$$\frac{\partial E(x,y)}{\partial \hat{g}(x,y)} = \sum_{r=1}^{m} \sum_{(k',l')\in\vartheta_{(k,l)}} \frac{(\hat{I}^r(k',l') - I^r(k',l'))}{\sigma_e^2} \times H_w \hat{R}(x,y) + \sum_{(x',y')\in\nu_{(x,y)}} \frac{(\hat{g}(x,y) - \hat{g}(x',y'))}{\sigma_g^2} \tag{16}$$

$$\frac{\partial E(x,y)}{\partial \hat{z}(x,y)} = \sum_{r=1}^{m} \sum_{(k',l')\in\vartheta_{(k,l)}} \frac{(\hat{I}^r(k',l') - I^r(k',l'))}{\sigma_e^2} \times H_w \hat{g}(x,y) \frac{\partial \hat{R}(x,y)}{\partial \hat{z}(x,y)} + \sum_{(x',y')\in\nu_{(x,y)}} \frac{(\hat{z}(x,y) - \hat{z}(x',y'))}{\sigma_z^2} \tag{17}$$

where from Eq. (3), $\frac{\partial \hat{R}(x,y)}{\partial \hat{z}(x,y)}$ is given by:

$$\begin{aligned}\frac{\partial \hat{R}(x,y)}{\partial \hat{z}(x,y)} &= \left(\ell_x \frac{p'_{xy}}{p_{xy}} + \ell_y \frac{q'_{xy}}{q_{xy}}\right) \frac{\vec{n}.\vec{s}}{\sqrt{p_{xy}^2 + q_{xy}^2 + 1}} \\ &\quad - \left(s_x \frac{p'_{xy}}{p_{xy}} + s_y \frac{q'_{xy}}{q_{xy}}\right) \frac{\vec{n}.\vec{\ell}}{\sqrt{p_{xy}^2 + q_{xy}^2 + 1}} \\ &\quad - (p'_{xy} + q'_{xy}) \frac{\vec{n}.\vec{\ell} \times \vec{n}.\vec{s}}{(p_{xy}^2 + q_{xy}^2 + 1)^{3/2}} \qquad (18) \\ p'_{xy} &= \frac{\partial p_{xy}}{\partial x} \quad \text{and} \quad q'_{xy} = \frac{\partial q_{xy}}{\partial y}.\end{aligned}$$

p_{xy}, q_{xy}, p'_{xy} and q'_{xy} are computed using the Prewitt operator.

4.2. *Computing $\hat{z}$ Using Local Cost Functions*

Newton's method can cause problems due to the non-convexity of the cost function for $\hat{z}$. In this section we propose a method, based on minimizing E by investigating its local variations. Assuming that variations in $\hat{z}$ at any pixel (x, y) can only cause local changes in E at each iteration (i.e., a Markovian property), we can calculate a descent direction by taking an average of local variations due to small changes ϵ at every pixel:

$$\begin{aligned}&\mathcal{E}\left\{\frac{E(\hat{z}(0,0),\ldots,\hat{z}(x,y)+\epsilon,\ldots,\hat{z}(D,D))}{\epsilon} - \frac{E(\hat{z}(0,0),\ldots,\hat{z}(x,y),\ldots,\hat{z}(D,D))}{\epsilon}\right\} \\ &\simeq \text{Avg.}\frac{\partial E}{\partial \hat{z}(x,y)} \qquad (19)\end{aligned}$$

where $\mathcal{E}$ denotes the expected value and Avg. implies the average. Computing (19) for every pixel would yield a correction vector $\nabla E_z = [\text{Avg.}\frac{\partial E}{\partial \hat{z}_{(0,0)}} \cdots \text{Avg.}\frac{\partial E}{\partial \hat{z}_{(D,D)}}]$. This is then accepted if the total cost is reduced at each iteration n by applying a relaxation with step size $\lambda^n \in [0, 1]$:

$$\hat{z}^{n+1} = \hat{z}^n + \lambda^n \nabla E_z, \quad \lambda^0 = 1 \tag{20}$$

Otherwise, the step size is reduced by half and the process is repeated until the relative reduction in E is smaller than a preset threshold value. A classical work in the use of this type of approach is carried out by Box and Wilson (1951). The computational cost is rather small due to the local nature of computations,

i.e., we only need to compute E in the neighbourhood of (x, y) which is given by $v_{(k,l)}$ and $v_{(x,y)}$.

Note that the same relaxation approach is used in the Newton's method or the deterministic gradient method by simply replacing ∇E_z by corresponding partial derivatives of E given by (16) and (17) for g or z. The use of (17) for computing z would, however, require an initialization near the solution.

5. Experimental Results

In this section we present some experimental results on both synthetic and real images. Mean Square Error (MSE) expressed as a percentage over the mean squared value of pixels in the ideal image has been used for measuring the quality of reconstructed images.

Figures 2(a) and (b) show the ideal high resolution synthetic albedo and altitude. The reconstructed high resolution albedo using Newton's method has been shown in Fig. 3. A set of four low resolution images (of which one has been shown in Fig. 2 (c)) was assumed to be available together with the assumption that the high resolution altitude is known.

Below are further synthetic images with results in Figs. 5 and 6.

Our study on real data was not, however, so straightforward, due to the lack of availability of albedo values and Digital Elevation Maps (DEM). It was, however, possible to investigate the proposed algorithm by generating a set of simulated aerial images, while taking the grey-scale image of the surface as being the albedo (see Fig. 7 for example). Reconstructed results are shown below in Figs. 8 and 9.

The algorithm was also tested on a SPOT satellite image (Fig. 10). This image was particularly difficult to handle, since it exhibits a considerable amount of fine details and discontinuities. Results, obtained using a set of simulated satellite images (as in the aerial image above) are given in Figs. 11 and 12.

6. Concluding Remarks

We presented, herein, an algorithm for recovering high resolution 3D information from a set of low resolution intensity images. It is important, however, to have interframe subpixel displacements (Irani and Peleg, 1989) so that pixel information incorporated in reconstructed images are obtained by data fusion. This, in practice, is equivalent to sampling the scene at a higher rate using a single high resolution camera. The advantage of the technique over pure interpolation is, therefore, the fact that the reconstructed image embodies interpixel values obtained directly from the actual scene using an error criterion, whereas in interpolation, interpixel values are computed using curve fitting techniques and carry no real information. Besides, change of spatial resolution is quite often obtained by trading the gray level quantization (Peleg et al., 1989).

Using Newton's Method allows for fast convergence of the algorithm for g. For z the Newton's method could only converge to the solution if the initialization was close enough to the solution. However, applying the method proposed in Section 4.2 produced good convergence properties. Results are indeed very much promising.

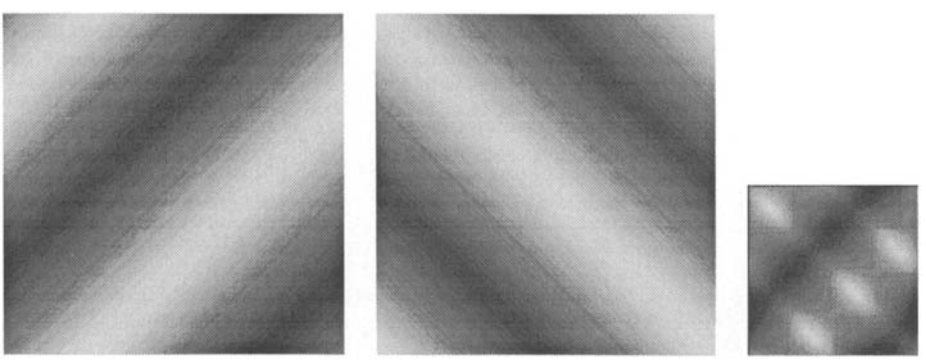

(a) (b) (c)

Figure 2. (a) High resolution albedo, (b) High resolution altitude, (c) One of 4 resolution camera images.

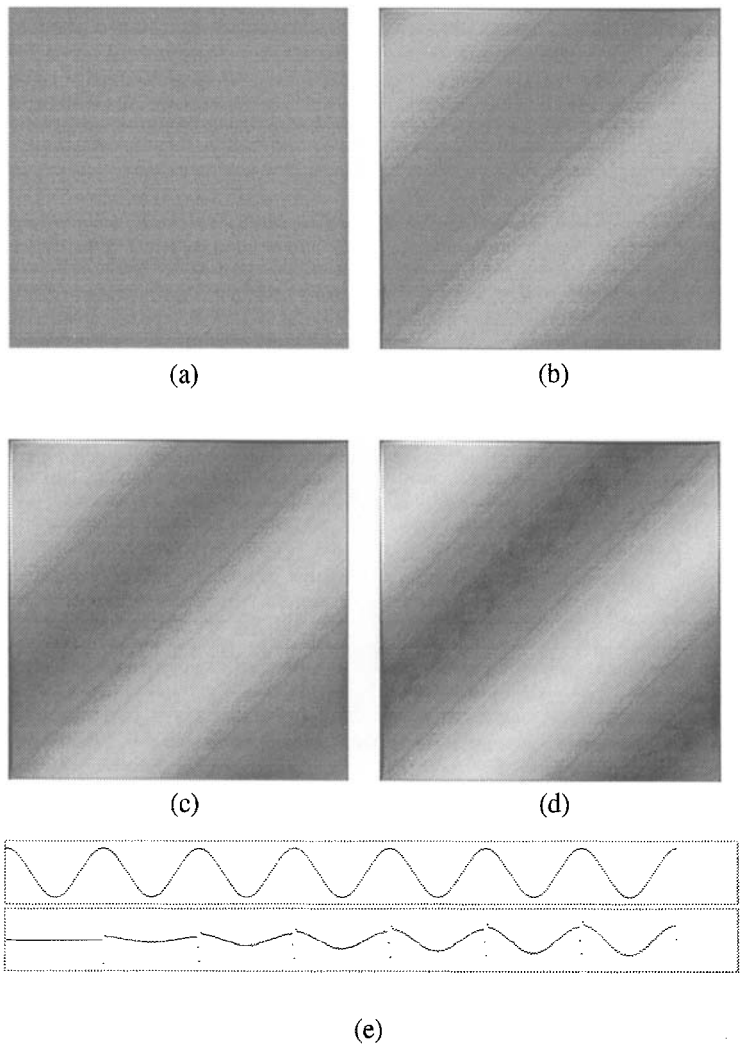

Figure 3. (a) Initialization, (b), (c) and (d) reconstructed albedo after 10, 20 and 30 iterations with MSE equal to 5.1%, 3.2% and 1.1% respectively, (e) a profile of a few iterations of the reconstruction compared to the ideal image.

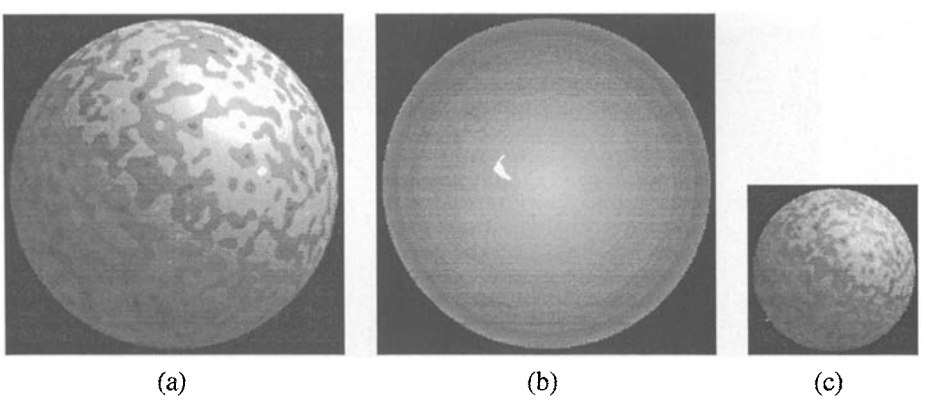

Figure 4. (a) High resolution albedo, (b) High resolution altitude, (c) One of 4 low resolution camera images.

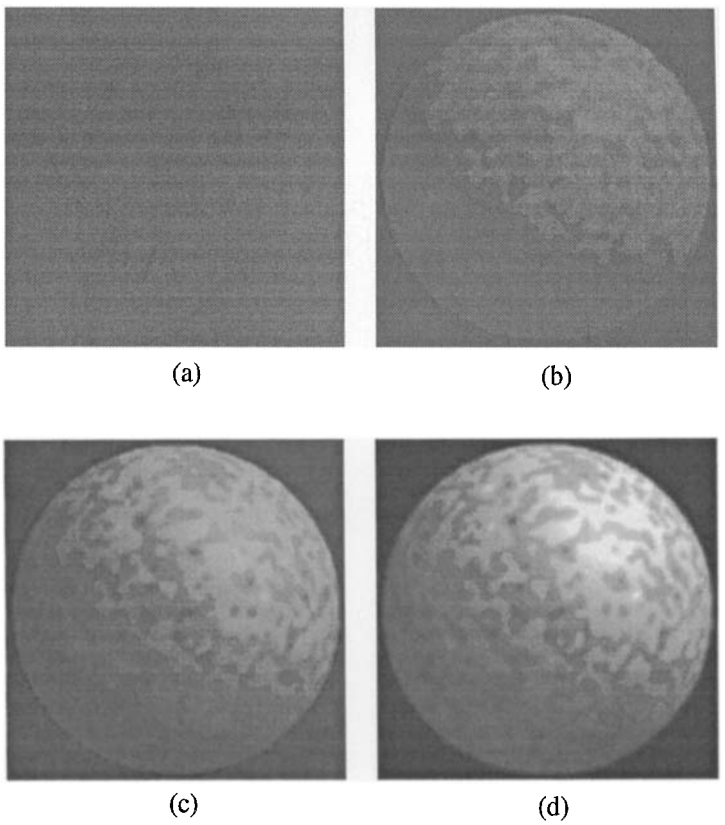

Figure 5. (a) Initialization, (b), (c) and (d) reconstructed albedo after 5, 20 and 70 iterations with MSE equal to 17.1%, 4.2% and 0.42% respectively.

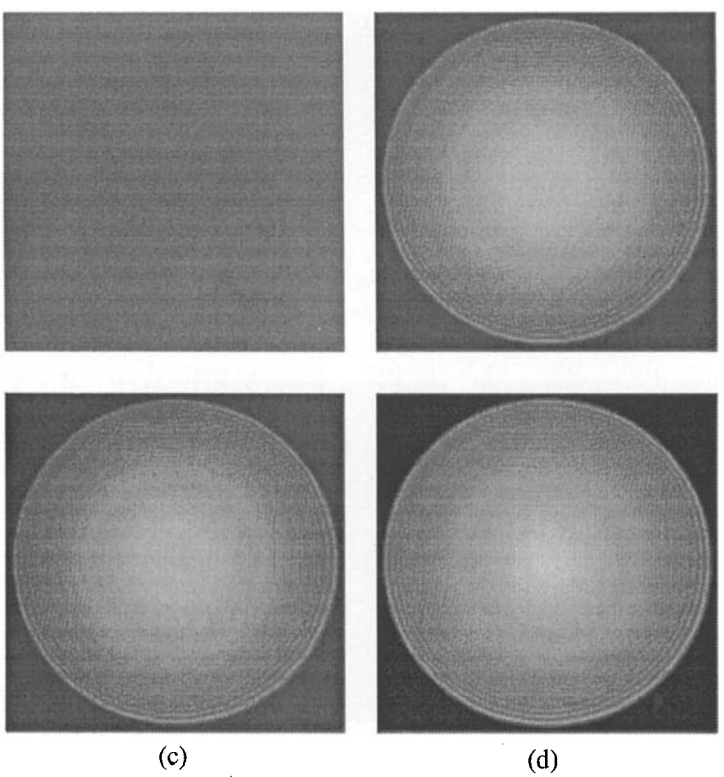

Figure 6. (a) Initialization, (b), (c) and (d) reconstructed height after 5, 10 and 22 iterations with MSE equal to 12.4%, 4.0% and 1.0% respectively.

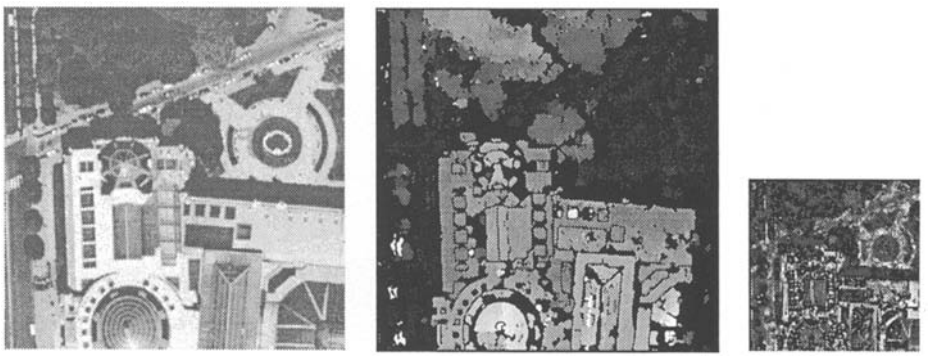

Figure 7. (a) High resolution albedo, (b) High resolution altitude, (c) One of 4 low resolution camera images.

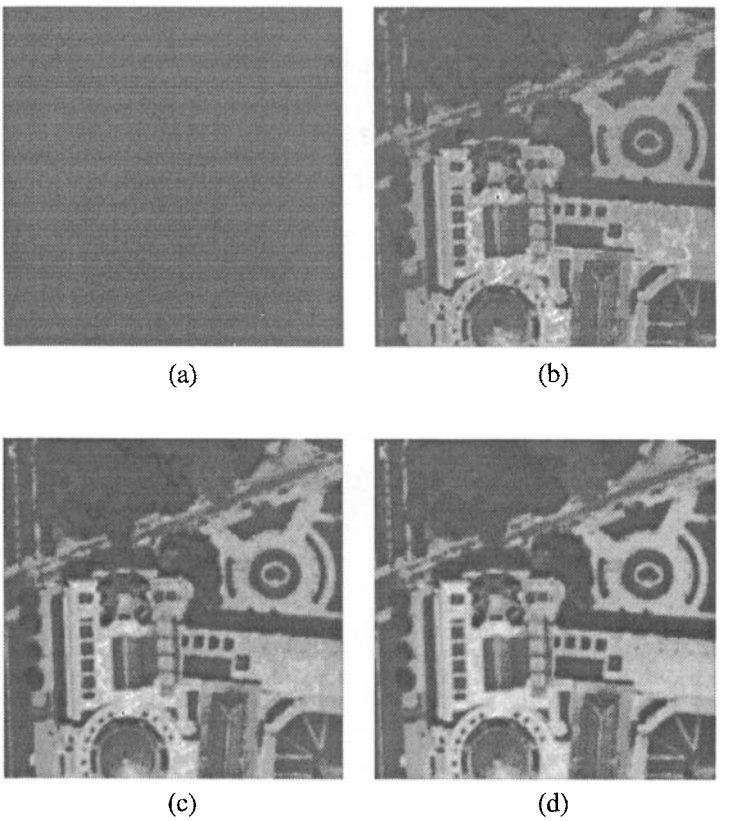

Figure 8. (a) Initialization, (b), (c) and (d) reconstructed albedo after 13, 26 and 39 iterations with MSE equal to 4.5%, 2.2% and 1.7% respectively.

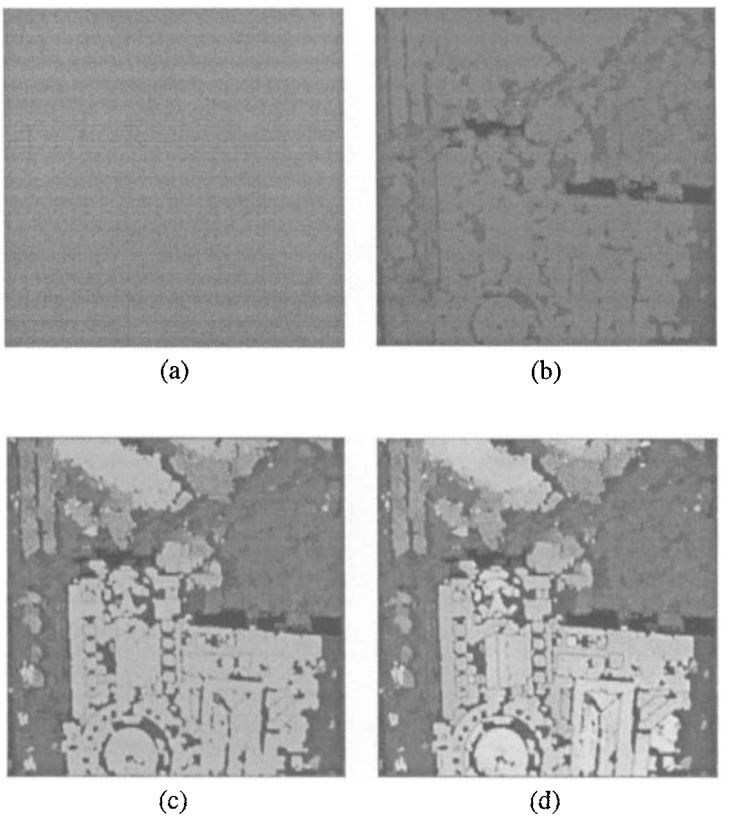

Figure 9. (a) Initialization, (b), (c) and (d) reconstructed height after 2, 10 and 15 iterations with MSE equal to 12.3%, 2.2% and 1.2% respectively.

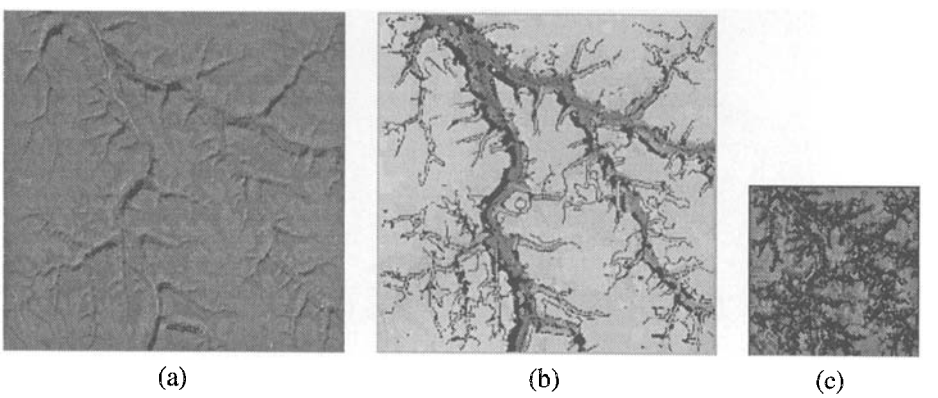

Figure 10. (a) High resolution albedo, (b) High resolution altitude, (c) One of 4 low resolution camera images.

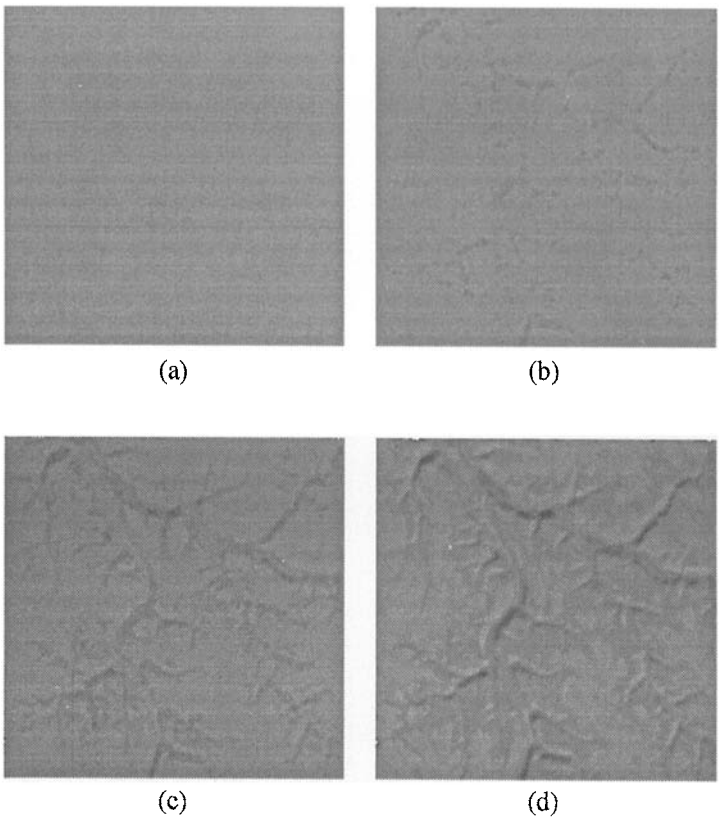

Figure 11. (a) Initialization, (b), (c) and (d) reconstructed albedo after 5, 10 and 70 iterations with MSE equal to 5.0%, 2.5% and 0.88% respectively.

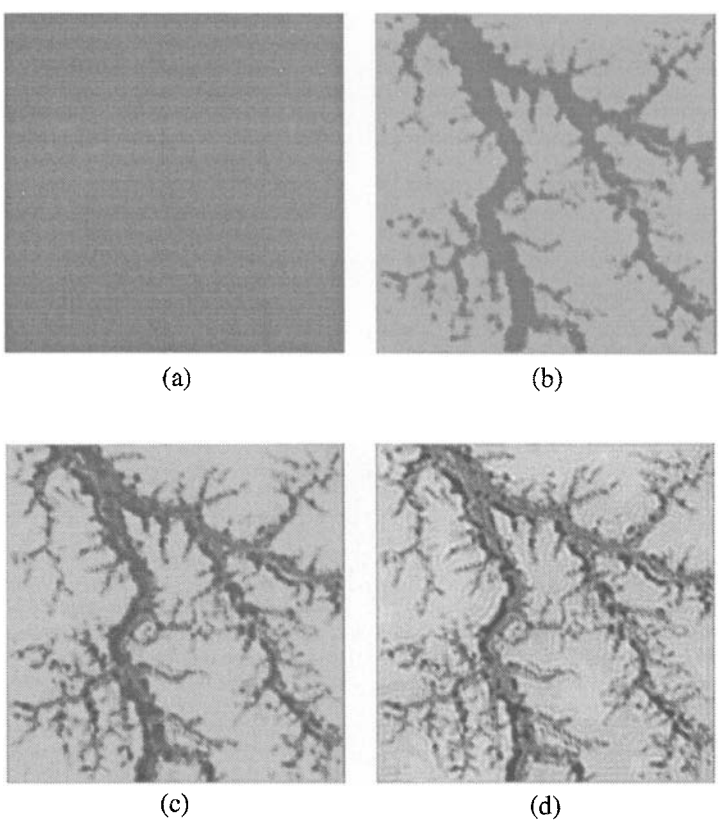

Figure 12. (a) Initialization, (b), (c) and (d) reconstructed altitude after 5, 10 and 15 iterations with MSE equal to 6.8%, 2.9% and 1.3% respectively.

In the case of real data, the choice of the relaxation parameter λ was found to be important not only for the speed of the convergence, but also for the quality of final results. Discretization prior to convolution can produce problems around the borders of the reconstructed images. These can be handled by means of extrapolation methods, assuming smoothness.

As for the resolution increase, the natural limit is obviously the Nyquist rate. Any increase beyond this rate of sampling would, therefore, be a pure interpolation contributed entirely by regularization.

In order to obtain better results, the algorithm will be extended by taking into account the discontinuities. Future extensions will also include simultaneous reconstruction of the albedo and height. The robustness of the algorithm to noise will also be scrutinized.

References

Andrews, H.C. and Hunt, B.R. 1977. *Digital Image Restoration*. Prentice-Hall Inc., 1st edition.

Azencott, R. 1987. Image analysis and Markov fields. *Proc. of Int. Conf. Ind. & Appl. Math*, SIAM, Paris.

Berthod, M., Shekarforoush, H., Zerubia, J., and Werman, M. 1993. Reconstruction of High Resolution 3D Visual Information, INRIA Research Report No. 2142, France.

Berthod, M., Shekarforoush, H., Zerubia, J., and Werman, M. 1994. Reconstruction of high resolution 3D visual information. *Proc. CVPR*, Seattle, Washington, pp. 654–657.

Besag, J.E. 1974. Spatial interaction and the statistical analysis of lattice systems (with discussion). *Jl. Roy. Statis. Soc.*, B 36:192–236.

Besag, J.E. 1986. On the statistical analysis of dirty pictures. *Jl. Roy. Statis. Soc.*, B. 48:259–302.

Blake, A. and Zisserman, A. 1987. *Visual Reconstruction*. MIT Press: Cambridge, MA.

Box, G.E.P. and Wilson, K.B. 1951. On the experimental attainment of optimum conditions. *Jl. of Roy. Stat. Soc.*, B. 13:1–45.

Bruss, A.R. 1982. The Eikonal equation: Some results applicable to computer vision. *Jl. of Math. Physics*, 23(5):890–896.

De Castro E. and Morandi, C. 1987. Registration of translated and rotated images using finite fourier transforms. *IEEE Trans. PAMI*, 9(5):700–703.

Frankot, R.T. and Chellappa, R. 1988. A method for enforcing integrability in shape from shading algorithms. *IEEE Trans. PAMI*, 10(4):431–451.

Geiger, D. and Girosi, F. 1991. Mean field theory for surface reconstruction. *IEEE Trans. PAMI*, 617–630.

Geman, S. and Geman, D. 1984. Stochastic relaxation, Gibbs distributions and the Bayesian restoration of images. *IEEE Trans. PAMI*, 6:721–741.

Gross, D. 1986. Super-resolution from Sub-pixel Shifted Pictures, Master's thesis, Tel-Aviv University.

Horn, B.K.P. 1970. Shape from shading: A method for obtaining the shape of a smooth opaque object from one view. Technical Report TR-79, Project MAC, MIT.

Horn, B.K.P. 1977. Understanding image intensities. *Artificial Intelligence*, 8(2):201–231.

Horn, B.K.P. 1989. Height and gradient from shading. *Proc. of Image Understanding Workshop*, DARPA.

Huang, T. and Tsai, R. 1984. Multiframe Image restoration and registration. *Advances in Computer Vision and Image Processing*, 1:317–339, JAI Press Inc.

Hutber, D. 1987. Improvement of CCD camera resolution using a jittering technique. *Proc. SPIE*, 849:11–17, Automated Inspection and High Speed Vision Architecture.

Irani, M. and Peleg, S. 1989. Super-resolution from image sequences. Technical Report 89-7, Dept. of Computer Science, The Hebrew University of Jerusalem.

Irani, M. and Peleg, S. 1991. Improving resolution by image registration. *Graphical Models and Image Processing*, 53(3):231–239.

Keren, D., Peleg, S., and Brada, R. 1988. Image sequence enhancement using sub-pixel displacement. *Proc. CVPR*, Ann Arbor, Michigan, pp. 742–746.

Keren, D. and Werman M. 1993. Probabilistic analysis of regularization. *IEEE Trans. PAMI*, 15:982–995.

Leclerc, Y.G. and Bobick, A.F. 1991. The direct computation of height from shading. *Proc. of CVPR*, Lahaina, Maui, Hawaii.

Marroquin, J., Mitter S., and Poggio, T. 1987. Probabilistic solution of ill-posed problems in computational vision. *Jl. of American Statistical Association*.

Moussouris, J. 1974. Gibbs and Markov random systems with constraints. *Jl. of Stat. Physics*, 10(1).

Peleg, S., Keren, D., and Schweitzer, L. 1987. Improving image resolution using subpixel motion, Pattern Recognition Letters, 223–226.

Peleg, S., Werman, M., and Rom, H. 1989. A unified approach to the change of resolution: Space and gray level. *IEEE Trans PAMI*, 11:139–141.

Prager, J. and Arbib, M.A. 1983. Computing the optic flow: The match algorithm and prediction. *Computer Vision Graphics and Image Processing*, 24:271–304.

Rosenfeld, A. and Kak, A.C. 1982. *Digital Picture Processing*. Vols. 1 and 2, 2nd ed., Academic Press Inc.

Terzopoulos, D. 1986. Regularization of inverse visual problems involving discontinuities. *IEEE Trans. PAMI*, 8(4).

Tikhonov, A. and Arsenin, A. 1977. *Solutions of Ill-Posed Problems*. W.H. Winston & Sons.

Wolff, L.B., Shafer, S.A., and Healey, G.E. 1992. *Radiometry, Physics Based Vision* (edited). Jones and Barlett Publishers.

Zerubia, J. and Chellappa, R. 1993. Mean field annealing using compound Gauss-Markov random field for edge detection and image estimation. *IEEE Trans. Neural Networks*, 4(4):703–709.